FULL PAPER

Unveiling the role of macrodipolar interactions in the properties of self-assembled supramolecular materials

Marina P. Oliveira,[a,b] Hans-Werner Schmidt,[c] and Rodrigo Q. Albuquerque*[b,d]

This paper is dedicated to Prof. Milton T. Sonoda (*in memoriam*)

Abstract: Self-assembling of supramolecules composed of benzene and cyclohexanetricarboxamide derivatives can form highly organized 1D fibers exhibiting macrodipoles. The way fibers pack in the condensed phase governs the final properties of the supramolecular material, where macrodipoles can be oriented parallel or antiparallel to each other, and their magnitude can be tuned by additional intra-columnar dipole stabilization. X-ray structural elucidation of these materials remains a real challenge due to the difficulty in growing single crystals. This problem can be tackled by using atomistic molecular dynamics to simulate supramolecular materials composed of cyclohexanetricarboxamide derivatives assuming different magnitudes and orientations of macrodipoles in the condensed phase, as we show here. The results provide insight on the isotropization mechanism of the supramolecules and also reveal that the relative orientation between macrodipoles can indeed influence their stability. This work nicely complements X-ray structural characterizations of supramolecular materials, and helps understand structure-property relationships of a range of similar non-covalent materials.

Introduction

The chemistry of molecular assemblies and the non-covalent bond,[1] or supramolecular chemistry, has seen remarkable development over the last decades,[2] giving us several functional supramolecular materials,[3,4] as well as promoting a deeper understanding of dynamical processes.[5,6] For instance. Haedler et al.[7] reported efficient long-range energy transport along self-assembled nanowires based on carbonyl-bridged triarylamines, which is suggested to be important for the development of organic nanophotonic devices. Coordination compounds with Pd(II) or Pt(II)[6,8–10] were also reported to self-assemble to form supramolecular polymers exhibiting ordered columnar phases.

[a] MSc. M. P. Oliveira
Laboratory of Physical Chemistry, ETH Hönggerberg
HCI, CH-8093 Zürich, Switzerland.
[b] Prof. Dr. R. Q. Albuquerque, MSc. M. P. Oliveira
São Carlos Institute of Chemistry, University of São Paulo
13560-970 São Carlos, Brazil.
[c] Prof. Dr. H.-W. Schmidt
Macromolecular Chemistry I, Bavarian Polymer Institute
University of Bayreuth, 95440 Bayreuth, Germany.
[d] Dr. R. Q. Albuquerque
School of Pharmacy & Biomolecular Sciences
Liverpool John Moores University, L3 3AF Liverpool, UK.
E-mail: R.Q.Albuquerque@ljmu.ac.uk

Supporting information for this article is given via a link at the end of the document.

A versatile class of compounds able to self-assemble into supramolecular columnar aggregates via threefold hydrogen bonding is based on tricarboxamide derivatives, specifically the 1,3,5-benzene- and 1,3,5-cyclohexanetricarboxamides (BTA and CTA, respectively). These compounds show considerably high thermal stability,[11] and some are known to form organogels[12] and hydrogels,[13–15] depending on the nature of the substituent. Furthermore, they are known to form intrinsic macrodipoles[16] due to the head-to-tail arrangement of the amide groups inside the columns, which plays an important role in intercolumnar interactions.[17,18] The ability to form macrodipoles made possible, among others, the alignment of supramolecular columnar BTA aggregates by applying an external electric field, which is of great interest for the development of novel memory devices.[19,20] The existence of macrodipoles has also been related to the ability of nanofibers to show electrical conductivity in just one direction.[21]

In the condensed phase of CTAs and BTAs, the macrodipoles of neighboring columns will interact with each other, which is thereby expected to influence the stability of the material. All three carbonyl groups of these supramolecular aggregates can point in the same direction, giving rise to the (3:0) conformation, or two of them could point e.g., upwards and the third downwards, whose conformation is represented by (2:1). In addition, the relative orientation between two supramolecular columns can be parallel or anti-parallel, which finally leads to four possible conformations for the whole supramolecular material, namely parallel-(3:0), antiparallel-(3:0), parallel-(2:1) and antiparallel-(2:1) (Fig. 1). Each of these four conformations can exhibit different macrodipolar interactions, which is expected to impact differently on the final stability and properties of the material. Typically, dipolar molecules are likely to orient themselves in an antiparallel arrangement, cancelling out the total dipole moment and increasing the stability in comparison to the parallel orientation, although other interactions might weaken this tendency.[22] Insight on macrodipolar interactions could be gained from inspection of the corresponding crystallographic structures, but the structural characterization of such materials at the atomic level is also very challenging because obtaining single crystals for X-ray experiments and sophisticated analysis of the Bragg reflections and diffuse scattering are demanding. Theoretical tools are therefore of great help to address this problem.

Molecular modelling tools are very important for understanding the structure-property relationship of systems, often addressing problems in an equally accurate yet easier or faster way than experiments. Several theoretical approaches have been used to study CTAs as well as BTAs. At the quantum mechanical level, Albuquerque *et al.* have used the semiempirical PM6 model to investigate the relation between the magnitude of the macrodipole and the supramolecular building block within a

column.[17] Additionally, the prediction of geometries and excited states of supramolecular columns[23] and the influence of the amide connection on the self-assembly of BTAs[24] have been studied at the Density Functional Theory (DFT) level. On the molecular mechanics level, the self-assembly of BTAs in a nonpolar solvent has been demonstrated using classical molecular dynamics (MD)[5,25] as well as coarse-grained simulations.[26,27] The reorientation of the macrodipole caused by an applied electric field, as well as the handedness of supramolecular columns of BTAs have been investigated using molecular dynamics simulations.[28]

To the best of our knowledge, atomistic simulations taking into account the influence of the macrodipolar interactions on the condensed phase of CTAs have not been performed. MD simulations of BTAs have already been carried out indicating the higher stability of (2:1) columns over (3:0), although the energy difference was reported to be small, in the range of 1 – 2 kcal/mol.[25] However, the influence of different types of arrangements of the amide groups, within and between columns, on the thermal stability and disassembly mechanism of the whole material has not yet been reported. MD simulations can predict the most stable conformation of CTA-based supramolecular materials at the condensed phase, as well as bring insight into their isotropization process, which was touched upon in an experimental paper by Schmidt *et al.*[11]

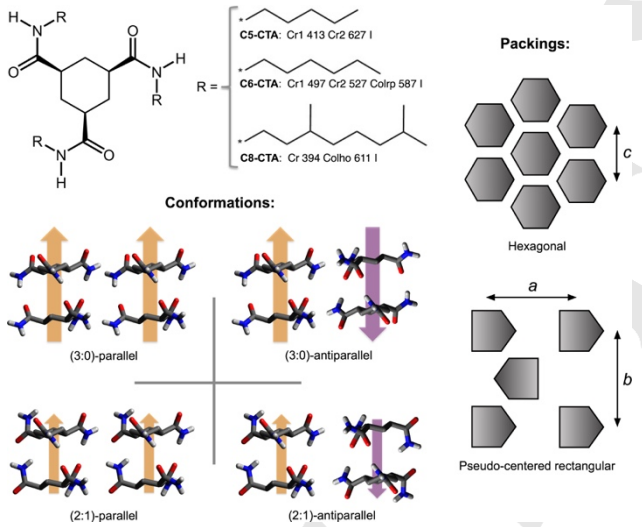

Figure 1. Monomer units investigated. conformations and packings adopted in the simulations. The corresponding experimental transition temperatures to the isotropic phase (= isotropization temperature, T_i, in K) are shown after each label, where Cr = crystalline, Col = columnar mesophase, I = isotropic, h = hexagonal, r = rectangular, p = plastic crystalline, o = ordered liquid crystalline. The arrows represent the macrodipoles of neighboring supramolecular columns in the condensed phase. *a*, *b*, and *c* are lattice parameters.

In this work, we aim to investigate the influence of the macrodipole-macrodipole interaction of CTAs at the condensed phase on their thermal stability by means of classical MD simulations. In addition, we want to get insight not only into the isotropization process, but also into the pre-isotropization process. To achieve this, different CTA derivatives selected on the basis of the availability of experimental data are used to build supramolecular columns (Fig. 1). CTA derivatives were chosen in this study in view of their much larger macrodipoles when compared with BTAs,[17] and also because the modelling of intracolumnar aromatic interactions becomes unnecessary. In order to calculate the properties of the assembled supramolecules, these are then treated using classical MD simulations. Finally, the results are compared with experimental data and the relation between thermal stability and macrodipole-macrodipole interactions is discussed.

Results and Discussion

This section is divided into three parts. In the first part, we discuss the ability of the force field to model the columnar arrangement of the investigated systems and show general trends of properties. In the second part, we show the results related to the transition temperatures from the columnar to the isotropic (disordered) phase and the role played by the relative orientation of macrodipoles. In the third part, we show the behavior of the material close to the isotropization point and during the isotropization process.

Validation of the interaction model and general trends

The comparison between the schemes used to generate partial charges initially used in the MD simulations is shown in Table S1, from where the Merz-Kollman scheme[29] was adopted for the rest of the simulations done here (Table S1, test number 9). The computed interdisc, intercolumnar and H-bonding distances of all simulated systems are shown in Fig. 2, where the RP and HP labels in the legend refer to pseudo-centered Rectangular Packing and Hexagonal Packing, respectively. The labels antiparallel and parallel (Fig. 1) were abbreviated in Fig. 2 as "Anti" and "Par", for simplicity.

Error bars were not shown in Fig. 2 because the standard deviations (*SD*) of the simulation triplicates were very small ($SD_{\text{intercolumnar\_distances}} \approx 0.001$-$0.01$ nm, $SD_{\text{interdisc\_distances}} \approx 0.001$-$0.002$ nm, $SD_{\text{H-bond\_distances}} \approx 0.001$-$0.003$ nm). While the predicted intercolumnar distances were independent of the conformation adopted and in excellent agreement with experimental data (for **C8-CTA** and **C6-CTA**), interdisc and H-bonding distances were strongly dependent on the intracolumnar arrangement. It has been shown[17] for similar non-covalent materials that (2:1) conformations have considerably more distorted columns and monomer units when compared to (3:0) ones, which might help understand why intracolumnar distances (H-bonding and interdisc) are conformation-dependent.

Although the MD simulations predict that (3:0) conformations have interdisc distances closer to the experimental values (Fig. 2. bottom), the absolute differences between the experimental and theoretical values for the (2:1) conformation is still small (0.08-0.17 Å) to rule out the latter conformation. The intercolumnar distances in general follow the same tendency presented by Tomatsu *et al.*,[30] in which they become smaller as the number of carbons in the side chain gets smaller (**C8-CTA** > **C6-CTA** > **C5-**

CTA). This suggests that our predicted value of about 1.35 nm for the intercolumnar distance of **C5-CTA** packed either in a HP (hexagonal packing) or RP (pseudo-centered rectangular packing) is reliable.

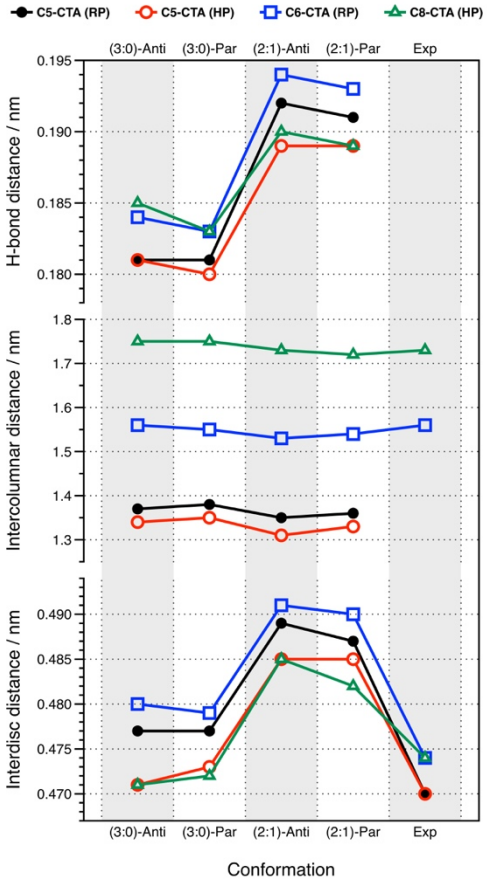

Figure 2. Influence of the intercolumnar and intracolumnar conformations on selected properties of the simulated materials. RP and HP refer to pseudo-centered Rectangular Packing and Hexagonal Packing, respectively. For more label details see Fig. 1.

Another difference between the (3:0) and (2:1) conformations is nicely revealed in Fig. 2. While one intuitively expects that only the latter conformation contributes to the stabilization of each single column due to the antiparallel arrangement of localized dipoles inside the same column, its slightly distorted geometry[17] weakens hydrogen bonding and increases the interdisc distances, as shown in Fig. 2. These counteracting effects, together with slightly different intercolumnar interactions must be taken into account to understand the final average energies computed for each conformation (Table S2). For instance, the potential energy for **C6-CTA** with antiparallel macrodipoles at 500 K is -2712 ± 0.08 and -2722 ± 0.11 kJ/mol for the (3:0) and (2:1) conformations, respectively. This energy difference is fairly small due to the discussed effects, but clearly shows that the (2:1) conformation is more stable. This is true in most cases, but for longer side chains (**C8-CTA**), where the larger intercolumnar distances slightly decrease the macrodipolar interactions, the (3:0) conformation is the most stable (Table S2). This trend indicates that for very long side chains, where in principle macrodipolar interactions could be neglected, the destabilization caused by the molecule distortion observed in (2:1) conformations overcomes the stabilization gained by the antiparallel arrangement of the localized dipoles inside each column, finally causing the (3:0) conformation to be lower in energy. Stabilization differences between these conformations seem to be therefore dependent on the length of the side chain. It is important to note that the (3:0) and (2:1) conformations can be interchanged by playing with the temperature (*vide infra*).

Some insight on the macrodipolar interaction can be gained based on the average potential energies calculated for all systems. Conclusions about this interaction can be drawn based on the RP packing only, since for the HP packing no noticeable difference between parallel and antiparallel arrangement of macrodipoles was found (Table S2). For **C5-CTA** (RP) in the (3:0) conformation, the antiparallel orientation between macrodipoles is about 4.7 kJ/mol more stable than the parallel one - this value changes to 4.2 kJ/mol in the case of the (2:1) conformation. For **C6-CTA** (RP), the same values are ca 9.6 and 6.4 kJ/mol for the (3:0) and (2:1) conformations, respectively. The corresponding standard deviations are rather small (0.04-1.23 kJ/mol), which means these small energy differences are meaningful. The energy trends suggest that *i)* the antiparallel orientation among macrodipoles can increase the overall stability of the material, and *ii)* this overall stabilization is directly proportional to the magnitudes of individual macrodipoles, since the weaker macrodipoles present in the (2:1) conformation stabilize less the material than those of the (3:0) conformation.

According to the potential energies obtained for **C5-CTA** (Table S2), the RP packing is on average 20 kJ/mol more stabilized than the HP packing, independently of the conformation. The additional stabilization experienced by each of the 128 molecules inside the simulation box is still very small (= 20/128 = 0.16 kJ/mol, with standard deviations of 10^{-4}-10^{-3} kJ/mol) to rule out the HP packing. If the kinetic pathways from the single molecule to the RP and HP packings are similar, one would then expect that **C5-CTA** would exhibit the thermodynamically more stable RP packing.

Figure 3 shows MD snapshots obtained for different compounds in different conformations and packings, visualized with (a,d) and without (b,e) periodic boundary conditions. The macrodipoles are represented by the wide arrows in Figs 3c,f. Figs. 3d,e reveal that the alkyl chains in the pseudo-centered rectangular packing are much better organized than those in the hexagonal packing (Figs. 3a,b). When the supramolecular columns are packed into a rectangular lattice they tend to minimize the void volume,[30] resulting in higher densities for the RP packing, independently of the conformation (Fig. S1). Another difference between both these packings is readily seen from their radial distribution functions (RDFs) involving the intercolumnar distances, which are shown in Fig. 4 for all compounds and conformations.

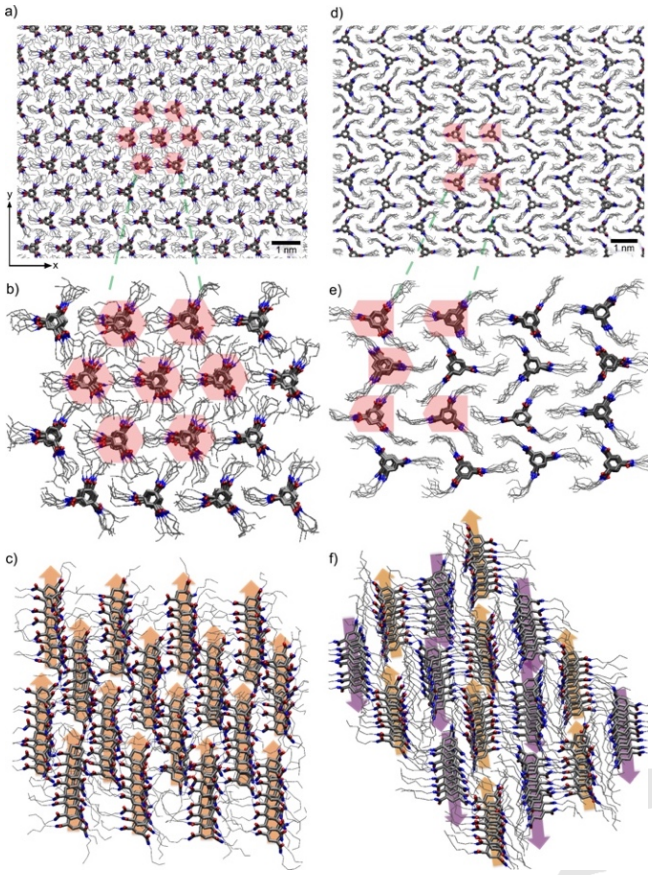

Figure 3. Different views for the packing of **C5-CTA** (HP) (a-c) and **C6-CTA** (RP) (d-f) within the (3:0)-parallel and (3:0)-antiparallel conformations, respectively, obtained from MD at 400 K and 1 atm. The upper structures (a,d) were built using periodic boundary conditions, and the zoomed ones in the middle are the respective simulation boxes highlighting the hexagonal (b) versus pseudo-centered rectangular (e) lattices. The relative orientation of macrodipoles (large arrows) is shown at the bottom structures (c,f).

The labels *a*, *b*, and *c* in Fig. 4 correspond to the lattice parameters shown in Fig. 1 and the red dotted lines represent the experimental lattice parameters. More values of the RDF peaks predicted for interdisc and hydrogen-bonding distances are shown in Table S3. The much larger number of RDF peaks obtained for the RP packing (Fig. 4) in general reflects its lower symmetry compared with the HP one. Even though the RP packing seems to be more organized than the HP one when one inspects the alkyl chains (compare Figs 3a and 3d), the carbons of the central ring of each compound used to build the RDF curves of Fig. 4 are more organized (or symmetric) for the HP packing.

For **C6-CTA**, the predicted *a* parameters were in excellent agreement with the experimental value,[30] while *b* was slightly smaller than expected. For **C8-CTA** the agreement between theoretical and experimental lattice constants is also excellent. These results strongly suggest that our predicted *a* and *c* parameters for **C5-CTA** (RP) and **C5-CTA** (HP), respectively (see Fig. 4), are very reliable, while a small correction factor could be applied to *b* to reproduce the same shift observed for **C6-CTA**.

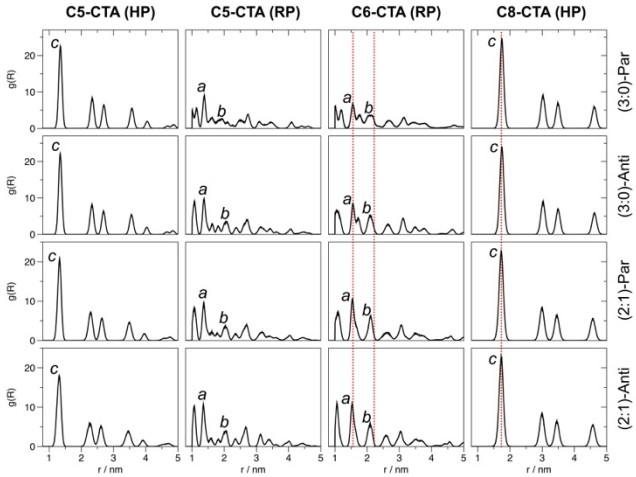

Figure 4. RDF plots involving the intercolumnar distances of the investigated materials under different conformations simulated at 500 K and 1 atm. The labels *a*, *b*, and *c* correspond to the predicted lattice parameters shown in Fig. 1 and the red dotted lines represent the experimental lattice parameters.

The transition temperature

The experimental phase transition temperatures to the isotropic state (isotropization temperature, T_i, see the experimental section for its definition) of the CTAs range from 587 K to 627K (Fig. 1). In this section, we demonstrate and discuss the predicted values for all compounds and conformations (Fig. 5).

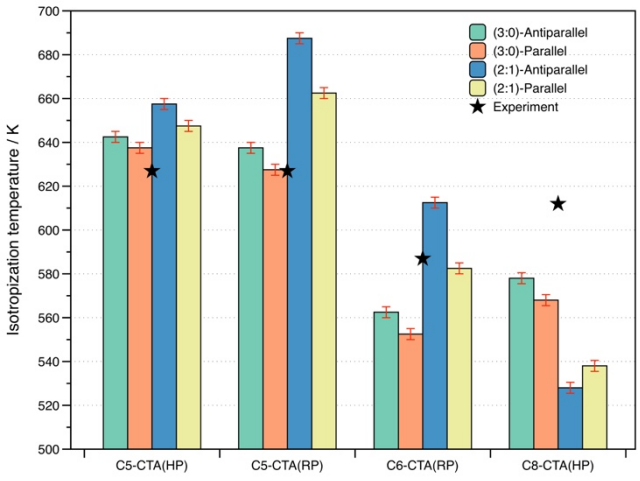

Figure 5. Isotropization temperatures (T_i) predicted for all compounds under different conformations and packings.

It is important to note that upon heating up the systems, the small energy barrier related to amide inversion (ca 1.5 kcal.mol^{-1})[28] can be overcome, meaning that some of the supramolecular columns of a system initially labelled as (3:0) could have some of its supramolecular columns in the (2:1) conformation at

temperatures close to T_i and vice-versa. This pre-isotropization process is discussed in more detail in the next section.

The higher the T_i value, the more thermodynamically stable is the respective system. It is clear from Fig. 5 that antiparallel conformations are always more thermodynamically stable than parallel ones independently of the relative orientations of the amide groups, namely (3:0) or (2:1). Macrodipole-macrodipole interactions seem to play a role in the stabilization of such supramolecular materials, since all of them have higher T_i values when their macrodipoles are antiparallel. This trend is also in line with the potential energies shown in Table S2.

For the same packing motif and conformation, increasing the size of the alkyl chains tends to decrease T_i (Fig. 5), which again emphasizes the stabilization gained from intercolumnar (or macrodipole-macrodipole) interactions, since only these interactions depend on the intercolumnar distance. This is in partial agreement with experimental findings, which reported the decrease of T_i upon increasing the length of the linear side chains containing 4-6 carbons,[11] while for even longer linear side chains the experimental T_i reaches a plateau and then it slightly increases again. Longer intercolumnar distances can surely decrease macrodipole-macrodipole interactions and therefore the overall stabilization, as already discussed, but this also stabilizes the system via intracolumnar and intercolumnar side chain interactions. Considerably longer side chains also hamper the formation of the isotropic phase by hindering molecular diffusion. This might explain why the experimental T_i of the 10-carbon side chain, branched **C8-CTA** was higher than that of **C6-CTA**.

The most thermodynamically stable (2:1)-antiparallel conformation (blue bars, Fig. 5) reproduces the trend in experimental T_i values discussed above for **C5-CTA** and **C6-CTA** only, but according to this conformation T_i would further decrease for **C8-CTA**, which disagrees with the experiment.[11] It is worth to say that, even though a certain conformation is predicted to be the most thermodynamically stable, this conformation might not be experimentally observed simply because the self-assembling process leading to it could be kinetically unfavorable, i.e., extremely slow. In this case, a less thermodynamically stable, but kinetically favored conformation could be self-assembled instead. Kinetic effects become gradually more important for longer or more branched side chains, since this directly decreases diffusion of monomer units during the self-assembling (or disassembling) process. The influence of kinetic effects on the self-assembly of the supramolecular systems investigated here could be only studied by using very long simulation times, which is the realm of coarse grained models, being out of the scope of this paper. However, the combination of the theoretical characterizations and experimental data can be used here to get insight on the structure of the investigated supramolecular systems, as discussed below.

Predicting the structure of the simulated systems requires finding the conformation that exhibits the best compromise between the experimental and theoretical T_i and RDF data. The conformation with largest thermodynamic stabilization ($T_i\uparrow$), that reproduces the experimental trend observed for T_i (**C5-CTA** > **C8-CTA** > **C6-CTA**), and that gives the best prediction of interdisc distances (Fig. 2, bottom) is the (3:0)-antiparallel conformation (green bars in Fig. 5). This suggests that the (3:0)-antiparallel conformation is likely to describe the real structure experimentally observed for those materials. This is in agreement with a very recent investigation published by one of the authors suggesting that neighboring supramolecular columns self-assembled from similar compounds with benzene cores exhibit antiparallel macrodipoles, and whose long range order is dependent on the nature of the side chains.[18] The analysis of the isotropization mechanism shown in the next section already assumes the (3:0)-antiparallel conformation as the starting structure for all compounds.

While both the packing motifs of **C5-CTA** have exhibited roughly the same predicted T_i for the (3:0)-antiparallel conformation (see Fig. 5), the theoretical RDF peak related to interdisc distances of the HP packing (4.72 Å) is in better agreement with the experimental value of 4.70 Å than the RP packing (4.78 Å), which suggests that hexagonal packing would be preferred over the pseudo-centered rectangular packing for **C5-CTA**.

Isotropization mechanism

When the temperature of the simulation is slightly below T_i, each system begins to increase its disorder, where columns start to bend, amide groups begin to rotate and invert, the restricted rotational motion of monomers inside columns become more pronounced, among others. For most of the systems at a high enough temperature, and inside a few of the columns, amide groups rotate by 180 degrees, inverting the initial orientation of the carbonyl groups and interconverting to a certain degree the (3:0) and (2:1) conformations (Fig. S2). The (3:0) conformation of all compounds have shown the amide inversion, which occurred at slightly different temperatures, while inversion of amides belonging to the (2:1) conformation was only observed for **C8-CTA** (Table S4). The inversion of amide/carbonyl groups caused by the alignment of the macrodipole of BTAs by means of an electric field has been previously investigated[19,20] and the mechanism involved in their ferroelectric switching has been elucidated using MD simulations.[28] The mechanism previously described for this process involves a sequence of three events: hydrogen bond breakage, bond rotation and formation of new hydrogen bonds. These events also summarize the process observed here, in which the conversion of carbonyl groups from one conformation, namely (3:0) or (2:1), to another was observed.

To get insight into the isotropization process, the angle between the (columnar) z axis and the line joining carbon and oxygen of each carbonyl group (Theta-OCZ), the number of hydrogen bonds, and interdisc and intercolumnar distances were monitored at T_i for all compounds initially in the (3:0)-antiparallel conformation, as shown in Fig. 6. The non-normalized ranges of the monitored properties are shown in Table S5. Note that the properties shown in Fig. 6 are meaningful during about the first half of the simulations: for instance, intercolumnar distances become very inaccurate when columns begin to disassemble. The isotropization process was much faster in the case of **C5-CTA**, as can be seen from the respective time scales in Fig. 6.

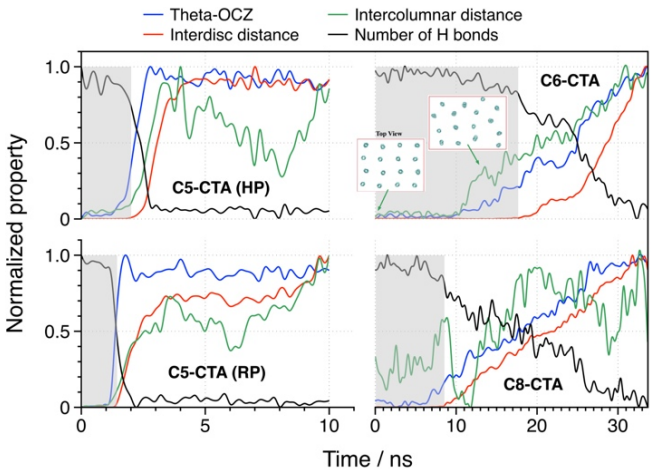

Figure 6. Variation of normalized properties during the transition at T_i from the columnar to the isotropic phase for systems in the (3:0)-antiparallel conformation. Theta-OCZ is the angle between the axis joining the carbon and oxygen atoms of the carbonyls and the z (columnar) axis. The highlighted grey regions correspond to the simulation time in which interdisc distances were still at their initial value. The inset (upper-right corner) is the simplified view of the simulation box along the z direction highlighting the changes in the intercolumnar order (watch the movie in the Supporting Information).

For all systems, the number of H bonds begins to oscillate while steadily decreasing during the whole phase transition (Fig. 6, black lines). These oscillations are related to periodic bond breakage and bond formation, whose processes are bridged by rotations of the amide groups, as previously discussed. Upon decreasing the number of hydrogen bonds, each monomer can rotate to a certain extent around the z-axis while most of the intracolumnar and intercolumnar ordering is unaltered. For all systems, rotational degrees of freedom (i.e., amide rotation and restricted monomer rotation relative to the z axis) are first added to the system in the beginning of the phase transition.

The highlighted gray regions in Fig. 6 correspond to the part of the MD simulation where interdisc distances (red lines) were at their initial values, meaning that all monomers were still building well-organized supramolecular columns. In all cases, one can see that the intercolumnar distances (Fig. 6, green lines) are oscillating and increasing while the intracolumnar monomers are kept at the same average distance from each other (Fig. 6, red lines). The oscillations are much stronger in the case of **C6-CTA** and **C8-CTA.** These trends indicate that the intercolumnar order is smaller than the intracolumnar order, which suggests that the second step in the phase transition is the formation of a transient nematic structure (Fig. 6, inset in the upper-right corner, watch the Supporting Information movie). Each transient structure is very short lived, being rather an intermediate species between the initial columnar and final isotropic phases, which co-exist at the same simulated temperature at least for a short period of time. This is in no contradiction with the fact that thermal properties of **C6-CTA** and **C8-CTA** investigated with thermogravimetric analysis and differential scanning calorimetry have not detected any transition from the columnar to the nematic phase,[11] but from the columnar to the isotropic phase. The class of materials investigated here do show transitions from columnar to isotropic phase via the nematic phase, but the latter needs to be thermodynamically stable over a *range* of temperatures to be experimentally observed.[11]

The magnitude of the oscillations in the intercolumnar distances (Fig. 6, green lines) inside the gray regions are directly related to the magnitude of macrodipole-macrodipole interactions. Since all systems are in the same (3:0)-antiparallel conformation, differences in macrodipolar interactions arise exclusively from the sizes of the alkyl chains, which controls the intercolumnar distance and therefore those interactions. **C5-CTA** has the smallest alkyl chain and consequently the smallest intercolumnar distance (see Fig. 4), meaning that it has the strongest macrodipole-macrodipole interaction. As a result, the corresponding supramolecular columns are relatively fixed with respect to each other, as can be in fact observed from the weak oscillations in the intercolumnar distances (Fig. 6, green lines inside the gray regions). If the length of the alkyl chains increases, as in **C6-CTA** or **C8-CTA**, supramolecular columns are much more loosely bound to each other because of the larger intercolumnar distance or weaker (less stabilizing) macrodipole-macrodipole interactions. This in turn increases the intercolumnar disorder, which nicely explains the stronger oscillations in the intercolumnar distances of **C6-CTA** and **C8-CTA**.

The last step is common to all systems and is intracolumnar in nature, consisting in the separation of the individual monomers to finally yield the isotropic phase (Fig. 6, red lines, outside the gray regions). In the case of **C8-CTA**, intracolumnar fragmentation has first led to the formation of smaller columns, e.g., dimers or trimers isotropically distributed, before a fully isotropic phase was reached. The considerably longer alkyl chains present in **C8-CTA** may have contributed to the stabilization of such small supramolecular columns due to the comparatively stronger van der Waals interactions involving the alkyl chains.

Conclusions

The present work has described the atomistic MD simulation of supramolecular materials exhibiting different inter- and intracolumnar conformations and strong macrodipoles, and has proposed a mechanism for the observed phase transition. The best partial charges used in the simulations were found by using the Merz-Kollman method using a pentamer previously optimized at the semiempirical level, and the CgenFF model was able to get a great insight on the properties of the simulated materials.

Stabilization differences between the (3:0) and (2:1) conformations have shown to depend on the length of the side chain, where the former is expected to be predominant in supramolecular materials with longer side chains. The antiparallel orientation among macrodipoles can increase the overall stability of the material, and this overall stabilization depends on the magnitudes of the individual macrodipoles, since the weaker macrodipoles present in the (2:1) conformation stabilize less the material than those of the (3:0) conformation, but this extra stabilization becomes less important when longer alkyl chains are

present, because of the associated increase in the intercolumnar separation. The comparison between experimental and theoretical RDF profiles and T_i trends suggests that the simulated supramolecular materials are likely to adopt the (3:0)-antiparallel conformation and that **C5-CTA** might adopt the HP packing.

The isotropization process of the investigated systems seems to occur in three steps, namely, initial H bond breakage leading to amide rotation and restricted monomer rotation around the columnar axis (step 1), formation of a transient nematic structure with high/low intracolumnar/intercolumnar order (step 2), and complete separation of the individual monomers caused by further breaking the H bonds to finally yield the isotropic phase (step 3). The magnitude of the oscillations in the intercolumnar distances for all the systems in the same (3:0)-antiparallel conformations were inversely proportional to the magnitude of macrodipole-macrodipole interactions.

The simulations and analyses carried out here are very useful to understand the stabilization and isotropization processes of other related supramolecular columnar materials and will surely contribute to the design of new non-covalent materials.

Experimental Section

Investigated Systems. Fig. 1 shows the three investigated compounds (**C5-CTA**, **C6-CTA**, **C8-CTA**), chosen because of the availability of experimental data related to the transition temperature, and interdisc and intercolumnar distances. The four possible conformations and packing motifs adopted here are also shown in Fig. 1. Note that the arrows (= macrodipoles) for 2:1 conformations are smaller because intra-columnar dipole-dipole stabilization takes place. Conformations with antiparallel columns are generally more stable than conformations with parallel columns, because of the stabilization between dipoles of opposite signs.[22] Experimentally, **C5-CTA** exhibits a transition from the crystalline to the isotropic phase,[11] but no crystallographic structure has been determined for this compound up to date, as well as nothing is discussed about the formation of supramolecular columns. Since the hexagonal and pseudo-centered rectangular lattices (Fig. 1) are the most common ways for tricarboxamides to self-assemble,[11,30] we have simulated **C5-CTA** adopting these two columnar arrangements with the purpose of investigating their influence on the material's properties and to try to get insight on the real packing motif. Finding the crystalline phase for **C5-CTA** is a much harder task and is out of the scope of this paper. For the other two compounds a pseudo-centered rectangular lattice for **C6-CTA**[30] and a hexagonal lattice for **C8-CTA**[11] were used. This information was used to build the initial configurations for all three compounds using the VMD program.[31] Since the experimental transitions shown in Fig. 1 for **C8-CTA** were measured for a racemic mixture, the simulations also used a racemic mixture of monomer units.

Interaction models. The topologies of CTA molecules were built using parameters from the CHARMM general force field, CgenFF.[32] Partial atomic charges were obtained from the ParamChem server[33] also based on the CgenFF model, and they were parameterized as follows. Partial atomic charges were computed by running 1 SCF (single point) calculations using Density Functional Theory (DFT) at the B3LYP/6-31-G(d) level of a pentamer column that was previously optimized at the semiempirical PM6 level. Initially different schemes for obtaining partial charges were investigated and the respective MD results were compared with experimental XRS data (Table S1), which led us to adopt the Merz-Kollman scheme.[29] Only the central monomer of the pentamer was selected to get representative partial charges in order to minimize border problems. The DFT and semiempirical calculations were carried out using the Gaussian09[34] and MOPAC,[35] respectively.

Simulations. All-atom MD simulations were performed for compounds **C5-CTA**, **C6-CTA**, and **C8-CTA** under periodic boundary conditions using a triclinic or rectangular box containing 4 by 4 columns of octamers, with a total of 128 monomers. This corresponds to 9600, 10752, and 15360 atoms for **C5-CTA**, **C6-CTA**, and **C8-CTA**, respectively. The equations of motion were propagated with the leap-frog algorithm using a time step of 1.0 fs. The Lennard-Jones interactions were treated via a smooth switching function starting at 12 Å with a cutoff of 14 Å, whereas electrostatic interactions were treated via the smooth particle mesh Ewald (PME) method[36] with a Fourier spacing of 0.1 nm. The cutoff adopted is appropriate to take into account non-bonded interactions between the polar amide groups belonging to neighboring columns, since the closest intermolecular O-O distance between two columns ranges from 7 Å (**C5-CTA**) to 11.5 Å (**C8-CTA**). The LINCS[37] algorithm was used to constrain all covalent bonds involving nonpolar hydrogens. The initial structures were energy minimized sequentially with the steepest descents and conjugated gradients methods until the maximum force was smaller than 100 kJ mol^{-1} nm^{-1}. The system was equilibrated by running MD simulations for 1.5 ns using the isothermal-isobaric (NPT) ensemble at 400 K and 1 bar and the Berendsen[38] algorithm with time constant of 2.0 ps for both thermal and barostat couplings. In the production phase, several MD simulations were carried out at different constant temperatures T and at 1 bar using the Nosé-Hoover thermostat[39,40] with coupling constant of 2.0 ps, and the Parrinello-Rahman barostat[41] with coupling constant of 3.0 ps. The duration of the production phase was 5 ns for temperatures T far from the transition temperature T_i, where $T_i - T > 10$ K, and 10 ns for simulations where $T_i - T \leq 10$ K. This procedure was done in triplicates for each system to increase statistical significance. In addition, 200 ns simulations were performed for **C8-CTA** at $T = T_i - 2$ K to confirm that no isotropization occurs before the predicted T_i value. All MD simulations were performed using the GROMACS 5.0.4 software package.[42]

Prediction of properties. Transition temperatures from the columnar to the isotropic phases, T_i, were determined by monitoring the potential energy and inter-molecular geometric parameters (intercolumnar and interdisc distances, number and length of hydrogen bonds, and angle formed between the carbonyl groups and the columnar z axis). The transition temperature was calculated according to $T_i = (T_{col} + T_{iso})/2$, where T_{col} is the highest temperature of the simulation in which the system remained self-assembled as columns and T_{iso} is the lowest temperature of the simulation in which the system melted to form the isotropic phase. Radial Distribution Functions, RDFs, were used to characterize the material and to assess the predictive capability of the interaction model used. RDFs for interdisc distances involved distances between the center of mass of the carbons of different central rings of all monomers, while RDFs for intercolumnar distances were calculated taking into account the x and y components of the distances among the center of masses of the carbons belonging to the central ring of each monomer. The RDFs for hydrogen bonds involved average distances between polar hydrogens and oxygens. The geometric parameters described above were monitored to get insight on the corresponding mechanisms of phase transition.

Acknowledgements

RQA would like to acknowledge the ECR-LJMU collaborative research project and the help of the technical training provided by the Finnish CSC-IT Center for Science in the frame of the PRACE (Partnership for Advanced Computing in Europe). HWS gratefully

acknowledges financial support from the German Research Foundation (SFB 840, B4). We are also indebted to Dr. Klaus Kreger for invaluable assistance and fruitful discussions.

Keywords: Supramolecular Chemistry • Non-covalent materials • Macrodipolar interactions • Molecular modelling

References

[1] J.-M. Lehn, *Eur. Rev.* **2009**, *17*, 263–280.
[2] J.-M. Lehn, *Chem. Soc. Rev.* **2007**, *36*, 151–60.
[3] M. Peplow, *Nature* **2015**, *520*, 148–150.
[4] A. Perrin, O. M. Musa, J. W. Steed, *Chem. Soc. Rev.* **2013**, *42*, 1996–2015.
[5] M. B. Baker, L. Albertazzi, I. K. Voets, C. M. A. Leenders, A. R. A. Palmans, G. M. Pavan, E. W. Meijer, *Nat. Commun.* **2015**, *6*, 6234.
[6] N. K. Allampally, M. J. Mayoral, S. Chansai, M. C. Lagunas, C. Hardacre, V. Stepanenko, R. Q. Albuquerque, G. Fernández, *Chem. Eur. J.* **2016**, *22*, 7810–7816.
[7] A. T. Haedler, K. Kreger, A. Issac, B. Wittmann, M. Kivala, N. Hammer, J. Köhler, H.-W. Schmidt, R. Hildner, *Nature* **2015**, *523*, 196–199.
[8] N. A. M. S. Caturello, Z. Csók, G. Fernández, R. Q. Albuquerque, *Chem. Eur. J.* **2016**, *22*, 17681–17689.
[9] M. J. Mayoral, C. Rest, V. Stepanenko, J. Schellheimer, R. Q. Albuquerque, G. Fernandez, *J. Am. Chem. Soc.* **2013**, *135*, 2148–2151.
[10] C. A. Strassert, C.-H. Chien, M. D. Galvez Lopez, D. Kourkoulos, D. Hertel, K. Meerholz, L. De Cola, *Angew. Chem. Int. Ed.* **2011**, *50*, 946–950.
[11] A. Timme, R. Kress, R. Q. Albuquerque, H.-W. Schmidt, *Chem. Eur. J.* **2012**, *18*, 8329–8339.
[12] K. Hanabusa, A. Kawakami, M. Kimura, H. Shirai, *Chem. Lett.* **1997**, *26*, 191–192.
[13] A. Heeres, C. Van Der Pol, M. Stuart, A. Friggeri, B. L. Feringa, J. Van Esch, *J. Am. Chem. Soc.* **2003**, *125*, 14252–14253.
[14] K. J. C. van Bommel, C. van der Pol, I. Muizebelt, A. Friggeri, A. Heeres, A. Meetsma, B. L. Feringa, J. van Esch, *Angew. Chem. Int. Ed.* **2004**, *43*, 1663–1667.
[15] A. Friggeri, C. van der Pol, K. J. C. van Bommel, A. Heeres, M. C. A. Stuart, B. L. Feringa, J. van Esch, *Chem. Eur. J.* **2005**, *11*, 5353–5361.
[16] A. Sakamoto, D. Ogata, T. Shikata, O. Urakawa, K. Hanabusa, *Polymer* **2006**, *47*, 956–960.
[17] R. Q. Albuquerque, A. Timme, R. Kress, J. Senker, H. W. Schmidt, *Chem. Eur. J.* **2013**, *19*, 1647–1657.
[18] C. S. Zehe, J. A. Hill, N. P. Funnell, K. Kreger, K. P. van der Zwan, A. L. Goodwin, H. W. Schmidt, J. Senker, *Angew. Chem. Int. Ed.* **2017**, *56*, 4432–4437.
[19] C. F. C. Fitié, W. S. C. Roelofs, M. Kemerink, R. P. Sijbesma, *J. Am. Chem. Soc.* **2010**, *132*, 6892–6893.
[20] C. F. C. Fitié, W. S. C. Roelofs, P. C. M. M. Magusin, M. Wübbenhorst, M. Kemerink, R. P. Sijbesma, *J. Phys. Chem. B* **2012**, *116*, 3928–3937.
[21] S. Yasutomi, T. Morita, Y. Imanishi, S. Kimura, *ScienceScience and Culture* **2004**, *304*, 1944–1947.
[22] S. Kimura, *Org. Biomol. Chem.* **2008**, *6*, 1143–1148.
[23] A. Bernet, R. Q. Albuquerque, M. Behr, S. T. Hoffmann, H.-W. Schmidt, *Soft Matter* **2012**, *8*, 66–69.
[24] P. J. M. Stals, J. C. Everts, R. De Bruijn, I. A. W. Filot, M. M. J. Smulders, R. Martín-Rapún, E. A. Pidko, T. F. A. De Greef, A. R. A. Palmans, E. W. Meijer, *Chem. Eur. J.* **2010**, *16*, 810–821.
[25] K. K. Bejagam, G. Fiorin, M. L. Klein, S. Balasubramanian, *J. Phys. Chem. B* **2014**, *118*, 5218–5228.
[26] K. K. Bejagam, S. Balasubramanian, *J. Phys. Chem. B* **2015**, *119*, 5738–5746.
[27] D. Bochicchio, G. M. Pavan, *ACS Nano* **2017**, *11*, 1000–1011.
[28] K. K. Bejagam, C. Kulkarni, S. J. George, S. Balasubramanian, *Chem. Commun.* **2015**, *51*, 16049–16052.
[29] U. C. Singh, P. A. Kollman, *J. Comput. Chem.* **1984**, *5*, 129–145.
[30] I. Tomatsu, C. F. C. Fitié, D. Byelov, W. H. De Jeu, P. C. M. M. Magusin, M. Wübbenhorst, R. P. Sijbesma, *J. Phys. Chem. B* **2009**, *113*, 14158–14164.
[31] W. Humphrey, A. Dalke, K. Schulten, *J. Mol. Graph.* **1996**, *14*, 33–38.
[32] K. Vanommeslaeghe, E. Hatcher, C. Acharya, S. Kundu, S. Zhong, J. Shim, E. Darian, O. Guvench, P. Lopes, I. Vorobyov, et al., *J. Comput. Chem.* **2009**, *31*, 671–690.
[33] "Parachem Server," can be found under https://cgenff.paramchem.org/, **n.d.**
[34] M. J. Frisch, G. W. Trucks, H. B. Schlegel, G. E. Scuseria, M. A. Robb, J. R. Cheeseman, G. Scalmani, V. Barone, B. Mennucci, G. A. Petersson, et al., *Gaussian 09, Rev. E.01, Gaussian, Inc., Wallingford CT*. **2009**.
[35] J. J. P. Stewwart, *Stewart Comput. Chem. HTTP//OpenMOPAC.net* **2016**.
[36] U. Essmann, L. Perera, M. L. Berkowitz, T. Darden, H. Lee, L. G. Pedersen, *J. Chem. Phys.* **1995**, *103*, 8577–8593.
[37] B. Hess, H. Bekker, H. J. C. Berendsen, J. G. E. M. Fraaije, *J. Comput. Chem.* **1997**, *18*, 1463–1472.
[38] H. J. C. Berendsen, J. P. M. Postma, W. F. van Gunsteren, A. DiNola, J. R. Haak, *J. Chem. Phys.* **1984**, *81*, 3684–3690.
[39] S. Nosé, *Mol. Phys.* **1984**, *52*, 255–268.
[40] Hoover, *Phys. Rev. A, Gen. Phys.* **1985**, *31*, 1695–1697.
[41] M. Parrinello, A. Rahman, *J. Appl. Phys.* **1981**, *52*, 7182–7190.
[42] M. J. Abraham, T. Murtola, R. Schulz, S. Páll, J. C. Smith, B. Hess, E. Lindah, *SoftwareX* **2015**, *1–2*, 19–25.